Biointerface Research in Applied Chemistry
Open-Access Journal (ISSN: 2069-5837)

Article
Volume 14, Issue 5, 2024, 121
https://doi.org/10.33263/BRIAC145.121

Enhancement of the Activity of Organophosphorus Hydrolase (OPH): An *in Silico* Approach using Docking, Molecular Dynamics Simulation, and MM-PBSA

Mostafa Akbariqomi [1], Taleb Badri [2], Mozafar Mohammadi [3], Said Yaghoob Sehri [4], Gholamreza Farnoosh [3,*]

[1] Tissue Engineering and Regenerative Medicine Research Center, Baqiyatallah University of Medical Sciences, Tehran, Iran; makbariqomi@gmail.com (M.A.);
[2] Neuroscience Research Center, Baqiyatallah University of Medical Sciences, Tehran, Iran; dr.badri52@gmail.com (T.B.);
[3] Applied Biotechnology Research Centre, Baqiyatallah University of Medical Sciences, Tehran, Iran; mohammadi8390@gmail.com (M.M.); rzfarnoosh@yahoo.com; (G.F.);
[4] Nephrology and Urology Research Center, Baqiyatallah University of Medical Sciences, Tehran, Iran; saidyaghoobsehri@yahoo.com (S.Y.S);
* Correspondence: rzfarnoosh@yahoo.com; (G.F.);

Scopus Author ID 55855454400
Received: 28.08.2023; Accepted: 23.11.2023; Published: 21.07.2024

Abstract: Enzymatic detoxification of Organophosphorus (OP) compounds such as nerve agents and some pesticides using enzymes is an ideal and promising approach to address environmental risks. Therefore, producing enzymes with high catalytic activity is necessary to degrade OP compounds. In this study, *in silico* methods have been studied to assess the effect of mutations in 176 and 184 residues of *Brevundimonas diminuta* Organophosphorus Hydrolase (OPH) in interaction with paraoxon. According to the molecular docking results, the binding affinity of the native enzymes, A176V, and L184M for paraoxon was -4.57, -4.6, and -4.6kcal/mol, respectively. Likewise, the hydrogen bond was formed in all three complexes between paraoxon and His 257. The 100ns Molecular Dynamic (MD) simulation study showed that the induced mutations have no negative effects on the protein structure's stability, folding, and flexibility. However, RMSF results indicate the possibility of strong and appropriate interactions between the ligand and some of the residues in mutant enzymes. Based on the Molecular-Mechanics Poisson-Boltzmann Surface Area (MM-PBSA) study, it was found that the higher free-binding energy (ΔGbind) was related to L184M, A176V, and native complexes, respectively; thus, L184M and A176V mutations increased the affinity of OPH to paraoxon. Among the energy components, the greatest effect on binding energy is related to polar solvation energy. The results of this computational study can be useful in the production of engineered OPH to increase catalytic efficiency and affinity to paraoxon.

Keywords: organophosphorus hydrolase; molecular dynamic; mutation; paraoxon; protein engineering.

1. Introduction

The high toxicity of Organophosphorus (OPs) compounds such as insecticides and Nerve Attenuation Syndrome (NAS) is related to their anticholinesterase activity, which suppresses the activity of acetylcholinesterase (AchE, EC 3.1.17) in the hydrolysis of cholinesterase (Ach) and terminates nerve stimulation at the site of neuronal synapses [1,2]. Therefore, these compounds are a serious hazard to the environment and humans. It is

necessary to develop efficient and appropriate detoxification methods for them. These methods must be safe, environment-friendly, and cost-effective, with a wide range of action [3]. Physical and chemical methods for decontamination of OPs are expensive and require special conditions [4]. An effective and safe alternative method is using organophosphorus-degrading enzymes. Identification of OPs-degrading enzymes such as microbial enzymes including Organophosphorus Acid Anhydrolase (OPAA) (EC 3.1.8.2), Methyl Parathion Hydrolase (MPH) (EC 3.1.8.1), SsoPox (EC 3.1.8.1), and Organophosphorus Hydrolase (OPH) (EC 3.1.8.1) have been researchers hopeful about using these green catalysts in the detection, destruction, and treatment of OPs poisoning [5,6].

OP degradation gene (opd) encodes OPH, which was first isolated from *Brevundimonas diminuta* MG (previously *Pseudomonas diminuta*) and *Sphingobium fuliginis* ATCC 27551 (previously *Flavobacterium* sp). The OPH is a 72-kDa homodimer metalloenzyme with two divalent cations in the active site, such as Zn^{+2}, Cd^{+2}, Co^{+2}, Ni^{+2}, or Mn^{+2}. This enzyme can break down P-O, P-F, P-CN, and P-S phosphorus bonds in various organic phosphorus compounds; thus, it is an enzyme with a broad substrate specificity [7]. However, the best substrate for this enzyme is paraoxon. The broad substrate specificity of the OPH makes it an excellent candidate for catalytic decontamination of organophosphorus chemicals. Notwithstanding, the catalytic properties of the OPH can be improved by protein engineering methods to use them more efficiently. The OPH's protein engineering targets include enzymatic catalysis, protein stability, stereoselectivity, and substrate preference [8].

Nowadays, computers and computational analysis play a vital role in many studies, especially in molecular biology. While experimental methods are laborious and time-consuming, *in silico* methods using the computer are both time and cost-effective [9]. Therefore, Molecular Docking, Molecular Dynamics (MD) Simulation, and Molecular Modeling (MM) methods can be used to obtain the degradation enzymes of the organophosphorus compounds with the desired properties [10]. For instance, MD simulation, MM-PBSA, and MM-GBSA analysis revealed that the reason for the stereochemical specificity of the PTE enzyme to SP-enantiomers is due to the closer interaction of His230 with paraoxon [11]. Mirzaei *et al*. (2015) used bioinformatics and MD simulation studies to increase the thermal stability of DFPase enzyme. The results show that Phe124Cys and Tyr305Cys mutation increase enzyme stability due to disulfide bond formation [12]. In another study on the DFPase enzyme using docking and MD simulation methods, it was found that the formation of disulfide bonds through V24C mutations with C76 amino acid increased the temperature stability of the DFPase [13]. The creation of disulfide bonds at some of the OPH enzyme sites was studied using rational design and *in silico* studies. Molecular and *in vitro* dynamics studies have shown that disulfide bonds increased the thermal stability of T128C/G153C and A204C/T234C mutant enzymes [14]. Investigation of methyl parathion hydrolase enzyme structure isolated from *Burkholderia jiangsuensis* illustrated that T64 was in the substrate-binding packet. In the native enzyme, only one hydrogen bond has been formed with A267 in the loop inside of the active site. In the T64N mutant enzyme, in addition to the hydrogen above bond, four hydrogen bonds with A25, G65, Y66, and P272 have been formed; thus, an enhancement of the polar bonds, enzyme structure stability, and enzyme-substrate interaction has been observed [15]. Molecular docking of the OPH isolated from *Acinetobacter* sp in the presence of the methyl parathion as substrate indicated that the I211A mutation reduced the size of the side chain and thereby created more space for movement of the flexible loop 10, which facilitated the movement of the loop and made it easier for the His157 on the loop to

approach the methyl parathion methoxyl group. The mentioned alteration resulted in a stronger interaction with methyl parathion in the mutant protein than in the native enzyme. This is because the mutation adjusted the structure near the binding pocket and stabilized the substrate-binding [16].

To increase the activity of OPH, we used a combination of *in silico* methods such as molecular docking, MD simulation, and MM-PBSA to design a novel mutant OPH with higher affinity and binding free energy to paraoxon.

2. Materials and Methods

2.1. Design and selection of mutations.

To determine the conservation of the target residues and choose the substitution amino acid, amino acid profiles of the selected positions were investigated using the Homology-driven Secondary Structure Prediction (HSSP) database. The HSSP is a database consisting of an alignment of homolog sequences of known 3D structures in PDB database [17]. It is a derived database by merging structural (3-D) and sequence (1-D) information. Modeller ver. 9.11 has been used to generate interesting mutations. For the mentioned purpose, OPH (1HZY) structure has been applied as a modeling template. Among the created models of each mutated enzyme, the best model was selected based on the lowest score of Discrete Optimized Potential Energy (DOPE) [18].

2.2. Molecular docking.

The best OPH substrate found to date is the paraoxon. The paraoxon structure was downloaded from the PubChem [19] database and converted into PDB format using Discovery Studio software. Preparation of the ligand was carried out using AutoDock Tools (ATD), and during the process, gasteiger charges were added to the ligand. Then, the final files have been saved in PDBQT format. Preparation of native and mutant OPH structures was performed to simulate docking using ADT. This preparation involves adding hydrogen atoms and Kollman charges to the protein and merging the non-polar hydrogen. Finally, the structures were saved in PDBQT format.

AutoDock 4.2 software has been applied to analyze molecular docking. Conformation with the least energy has been considered the best binding conformation between ligand and protein [20]. Using this software requires the preparation of two files named gpf (Grid Parameter File) and dpf (Docking Parameter File). The gfp file provides three-dimensional searching space for all ligand atoms by determining three-dimensional points in the selected grid and their spacing. The grid size was set to 126, 126, and 126Å for X, Y, and Z, respectively. The distance between the grid points was considered to be 0.175Å. The center of the grid for X, Y, and Z was 46.581, -3.019 and 27.29Å, respectively. The dpf file contains information on the algorithm applied to the docking process. This file was generated using the Lamarkin Genetic Algorithm (LGA). Docking parameters include a population size of 150, a maximum number of evaluations of 2,500,000, a maximum number of generations of 27,000, a maximum number of the top individuals that automatically survived 1, a gene mutation rate of 0.02, and a crossover rate of 0.8 [20]. Enzyme and substrate interaction was illustrated in 2D and 3D using LigPlot + V.1.4.5 [21] and Discovery Studio Visualizer software, respectively.

2.3. Molecular dynamics simulation.

The docked complexes were subjected to MD simulations using GROMACS 5.0.7 with topologies of native and mutant OPH generated using the GROMOS96 53a6 force–field parameters [22]. Inanition PRODRG server was utilized to prepare the ligand topology file. After successfully generating the topology files, the Simple Point Charge (SPC) model was used for water molecules. The system's total charge was then neutralized by adding sodium and chloride ions as required. One thousand steepest descent energy minimization steps were carried out without constraints to minimize the system's energy. After energy minimization, the equilibration of the system was made in two phases: first, NVT (constant number of particles, volume, and temperature) equilibration, with constant temperature (300K) for 100ps; second, an NPT (constant number of particles, pressure and temperature) equilibration with constant pressure of 1 bar and constant temperature of 300K also for 100ps. Finally, a 100ns MD simulation was executed on the equilibrated system, and final structures were extracted for further analysis. All the trajectory files were analyzed using the trajectory analysis module embedded in the GROMACS simulation package. The trajectory files were analyzed by using gmx confirms, gmx rmsd, gmx rmsf, gmx gyrate, gmx sasa and gmx hbond GROMACS utilities to extract the graph of Root-Mean-Square Deviation (RMSD), Root-Mean-Square Fluctuation (RMSF), Radius of gyration (Rg), and Hydrogen bond (H-bond).

2.4. MM-PBSA energy analysis.

The g_mmpbsa is a GROMACS tool that implies the Molecular Mechanics/Poisson-Boltzmann Surface Area (MM-PBSA) method to compute the ligand-free binding energies (ΔG_{bind}) [23, 24]. The g_mmpbsa tool calculates each parameter for the energy of protein and ligand in an aqueous solvent; therefore, it calculates the free energy of binding the ligand associated with the protein. The ΔG_{bind} of the protein-ligand complex in the aqueous solvent is given by the following equation:

$$\Delta G_{bind} = G_{complex} - (G_{protein} + G_{ligand}) \quad (1)$$

Where $G_{complex}$ is the energy of the protein-ligand complex, $G_{protein}$ and G_{ligand} are the energy of protein and ligand in an aqueous solvent, respectively. The free energy for each of the above is calculated as follows:

$$G_x = E_{bonded} + (E_{vdw} + Eelec) + G_{polar} + G_{non\text{-}polar} \quad (2)$$

$$G_{non\text{-}polar} = \gamma SASA + b \quad (3)$$

Where G_x (can be $G_{complex}$, $G_{protein}$, or G_{ligand}), E_{bonded} denotes the energy contributed by bonded interactions and is always equal to zero, whereas E_{vdw} is the van der Waals energy and E_{elec} is the electrostatic energy. G_{polar} is the electrostatic solvation-free energy, and $G_{non\text{-}polar}$ is the apolar solvation-free energy. Also, SASA is the solvent-accessible surface area, whereas γ is a surface tension coefficient, and b is the fitting parameter [24].

3. Results and Discussion

3.1. Generation of mutant's structures.

The HSSP has been applied to determine the conservation score of Alanine 176 and Leucine 184. The entropy for these positions was 1.36 and 0.83, respectively (Table 1). Entropy indicates the degree of conservation for the target site, and the lower entropy, the higher the conservation [17]. The type and frequency of amino acids related to the two positions, 176 and

184, are presented in Table 1. The results of HSSP showed that in position 176, 3% of the frequency was related to alanine, and the highest was related to Valine. At position 184, the highest frequency was related to leucine. In the selection of alternative amino acids, the frequency and the type of amino acids were considered. Alanine is a non-polar amino acid; thus, Valine, both non-polar and most abundant in this position, has been selected for the mutation (A176V). At position 184, methionine has been selected as an alternative amino acid instead of tyrosine (the most abundant and polar amino acid at position 184) because methionine is non-polar and the most abundant amino acid after tyrosine (L184M) (Table 1). The structure of mutant enzymes was generated with Modeller 9.11 software, and the best model for each structure was selected based on DOPE [18].

Table 1. HSSP analysis results for Ala176 and Leu184.

	V	**L**	**I**	**M**	**F**	**W**	**Y**	**G**	**A**	**P**	**S**	**T**	**C**	**H**	**R**	**K**	**Q**	**E**	**N**	**D**	**ENTROPY**
A176	46	17	26	7	0	0	0	0	3	0	0	0	0	0	0	0	0	0	0	0	1.364
L184	0	80	4	5	2	0	6	0	2	0	0	0	0	0	0	0	0	0	0	0	0.834

3.2. Molecular docking.

Molecular docking is a theoretical simulation method that analyzes the interaction and behavior of small molecules, such as ligands, at the active site of the enzyme and predicts binding modes and affinities based on computer analysis [25, 26]. Therefore, in the current study, molecular docking of native and mutant OPH with paraoxon was carried out using AutoDock 4.2 software. This software calculates torsional and internal energies and uses them to estimate the binding energy [27, 28]. The structure of the OPH is shown in Figures 1A and 1B, and the molecular docking results are shown in Figure 1C. Docking energy calculations are presented in Table 2 as well. Based on the results, it was found that the binding energy of paraoxon to OPH was -5.57kcal/mol, and the ligand with His257 formed a hydrogen bond with a length of 1.78Å. In the A176V complex, the ligand with energy -4.6kcal/mol is in the active site. In this complex, the hydrogen bond length between His257 and paraoxon is 1.64Å. The binding energy of the ligand to the L184M is -4.6kcal/mol. In this mutant, like the native enzyme, a hydrogen bond is formed between the ligand and His257, which is 2.68Å bond length (Table 2, Figure 1B). Hydrogen bonding plays an important role in the strong interaction of ligands and enzymes. A hydrogen bond was formed between the ligand and His257 in all three studied complexes. However, the length of this bond varies (A176V <WT <L184M). The shorter the hydrogen bond length, the stronger the bond. However, the binding energy in the natural OPH complexes and mutants with the ligand did not show a direct relationship with the length of the hydrogen bond, which could be related to the differences observed in other energies and effective bonds in binding paraoxon to the active site of the enzyme (Table 2). The intermolecular energy of each complex is determined by the amount of vdW + Hbond + desolv energy and electrostatic energy. Therefore, it is observed that the binding energy of paraoxon with A176V mutant, despite the shorter length of the hydrogen bond, is equal to the binding energy of paraoxon with L184M because the electrostatic energy in the L184M complex is less than the natural complex (Table 2). There are two Zn^{2+} in the active site of OPH, and the docking results indicate the presence of these ions in the active site (Figure 1B); thus, all three enzyme-ligand complexes are suitable for further analysis [29].

Table 2. List parameters generated from molecular docking showing the interaction behaviors of native OPH and its mutants with paraoxon.

Mutants	Native	A176V	L184M
Free energy of binding (kcal/mol)	-4.57	-4.6	-4.6
Inhibition constant (micromolar)	450.61	421.66	423.05
Intermolecular energy (kcal/mol)	-6.65	-6.69	-6.69
vdW + Hbond + desolv energy (kcal/mol)	-7.01	-7.31	-6.95
Electrostatic energy	0.35	0.61	0.26
Total internal energy (kcal/mol)	-0.82	-0.83	-0.48
Torsional energy (kcal/mol)	2.09	2.09	2.09

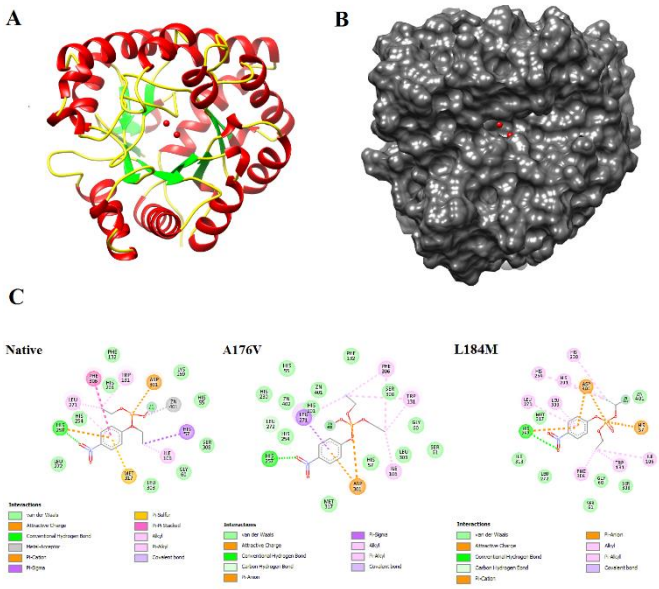

Figure 1. (A) A ribbon diagram of OPH monomer. The helices, the sheets, and the loops are colored red, green, and yellow, respectively. And the zinc atoms are shown as red spheres; **(B)** The surface representation of OPH. The surface of OPH is colored dark grey. The orientation of panels A and B are the same; **(C)** 2D diagram showing interactions between paraoxon and native and mutated OPH amino acid residues obtained from molecular docking simulation.

3.3. MD simulation of enzyme-ligand complexes.

Molecular docking methods are useful in determining potential binding modes but do not provide complete information about the stability of the structure and the interaction of ligands and enzymes. Therefore, MD simulations are used to learn the details of this interaction [30]. The MD simulation is a computational technique that increases awareness and understanding of structure configuration changes over a specified period. This information is necessary to predict the stability of the enzyme-ligand complex and the correct ligand binding and to calculate biological complexes' kinetic and thermodynamic properties [31]. Since MD simulation can provide a comprehensive analysis of the effect of mutations on protein structure, the OPH complex and mutant with paraoxon were investigated using a 100ns MD simulation trajectory. The data of this simulation were applied using different Gromex modules to study the RMSD, RMSF, Rg, H-bond, and MM-PBSA indices of enzyme-ligand complexes.

3.4. Root mean square deviation (RMSD).

The RMSD is a comprehensive measurement of protein variation used to investigate the dynamic stability of proteins and ligands over a period of time, which can be used in MD simulation studies [32]. The RMSD analysis was carried out to examine deviation pattern changes between the native OPH complex and the mutant with paraoxon, which showed that

the deviation was between 0.15 (nm) and 0.25 (nm) in the native complex. The average RMSD values in the native, A176V, and L184M complexes were 0.18nm (Figure 2). The equality of RMSD indicates the stability of these three complexes and that mutations do not hurt enzyme stability. Together, these results indicate the stable dynamic behavior of the structures during MD simulation (Figure 2). It is known that the lower the RMSD value, the better the fixation of the ligand in a suitable position in the protein-ligand complex.

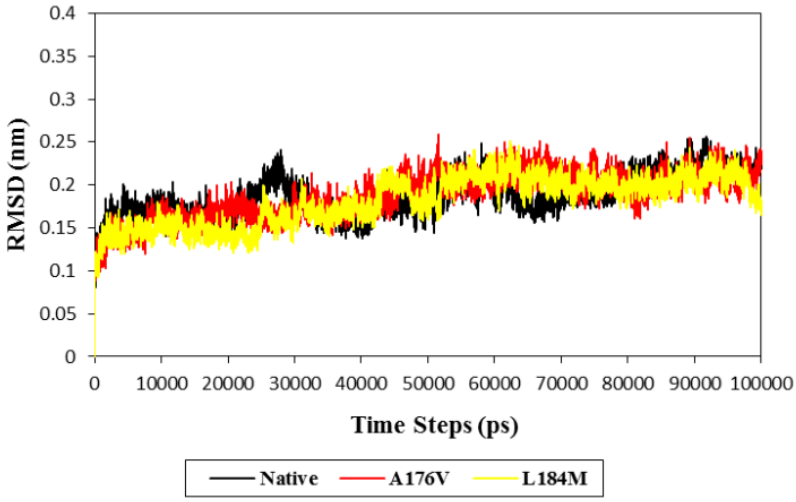

Figure 2. Time-dependent root-mean-square deviation (RMSD) of the OPH (native and mutants) and paraoxon complexes. Black, red, and yellow colors represent native/paraoxon, A176V/paraoxon, and L184M/paraoxon complexes, respectively.

3.5. Root mean square fluctuation (RMSF).

The RMSF analysis is performed to estimate the fluctuation of each residue during the simulation [33]. Although RMSD and RMSF are similar, the main difference is that RMSD exhibits molecular stability while RMSF exhibits flexibility changes [34]. The amount of RMSF indicates the flexibility and rigidity of the structure; thus, the parts of the structure that have high RMSF include turns, bends, and coils, while the low RMSF indicates rigid secondary structures such as alpha-helix and beta plates [35]. The RMSF analysis of native and mutant complexes confirms that the most conformational changes observed in these complexes are related to loops. Loops 1, 7, and 8, which include residues 59-77, 258-270, and 304-325, respectively, form the entrance of the active site (Figure 3) [36].

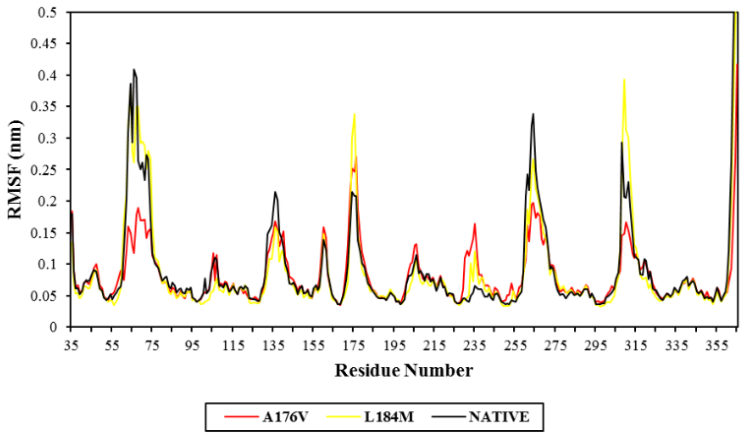

Figure 3. The root-mean-square fluctuation (RMSF) for OPH (native and mutants) and paraoxon complexes. Black, red, and yellow represent native/paraoxon, A176V/paraoxon, and L184M/paraoxon complexes, respectively.

Structural changes in these loops will likely cause tighter fitting of the paraoxon at the active site of the enzyme by widening the active site entrance [29]. The mean RMSF value of these three loops for the native complex is 0.22, 0.2, and 0.13nm, respectively. Likewise, in the A176V complex, the average RMSF value of loops 1, 7, and 8 is 0.1, 0.14, and 0.10nm, respectively. The fluctuation changes of the mentioned loops in the L184M complex are 0.22, 0.16, and 0.13nm, respectively (Figure 3). It should be noted that the binding of the ligand reduces the fluctuation rate of residues with strong interaction with the ligand or adjacent to the ligand. It seems that the relative reduction in the fluctuation of the residues of these three loops in mutant complexes is due to more or stronger bonds of the residues in the active site with paraoxon.

3.6. Radius of gyration (Rg).

The stability of each complex was further evaluated by calculating the radius of gyration. The radius of gyration can provide functional information about the amount of folding or compaction level of the protein-ligand complex [37]. The higher the Rg rate, the lower the compaction [38]. The mean Rg of the native complexes and mutants is 1.9nm (Figure 4). Although the Rg of the A176V complex has fluctuated somewhat at times, it is in a constant range and confirms the stability of the complex. According to these results, the radius of the hydrodynamic gyration of mutant structures has not changed compared to the native (Figure 4).

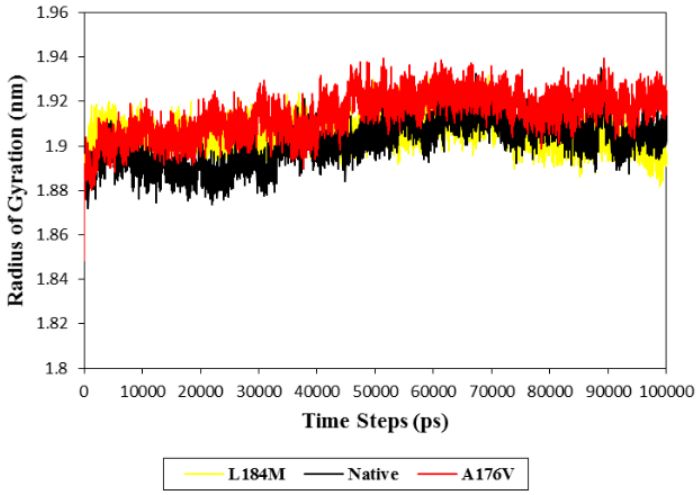

Figure 4. Plot of radius of gyration vs. time for OPH (native and mutants) and paraoxon complexes. Black, red, and yellow colors represent native/paraoxon, A176V/paraoxon, and L184M/paraoxon complexes, respectively.

3.7. Hydrogen bond (H-Bond).

Hydrogen bonds are the most important weak interactions observed in chemistry and biology. A hydrogen bond occurs when a hydrogen atom covalently attached to a molecule interacts with an electronegative atom of the same molecule or other molecules. In nature, hydrogen bonds play an important role in molecular recognition and stability of protein structure [34, 39]. The high number of intermolecular hydrogen bonds increases the stability of the protein-ligand complex [40]. Therefore, in this study, the number of hydrogen bonds between paraoxon and OPH native and mutant structures was calculated using the hbond gmx module and based on the distance of 3.5Å and cutoff angle of 30 (Figure 5). This analysis showed that for the native complex, A176V, and L184M mutants, the number of hydrogen

bonds reached three and in most cases shows one or two bonds (Figure 5). Based on these results, the interaction between enzyme and substrate is stable in all complexes.

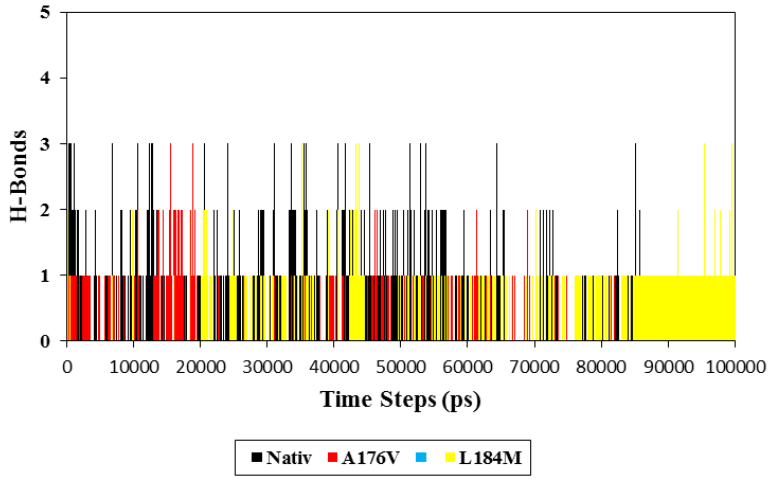

Figure 5. A number of hydrogen bonds were calculated to evaluate protein-ligand interaction with respect to the time of the OPH (native and mutants) and paraoxon complexes. Black, red, and yellow colors represent native/paraoxon, A176V/paraoxon, and L184M/paraoxon complexes, respectively.

3.8. Binding free energy calculation: MM/PBSA.

To better understand the effect of applied mutations in the structure of OPH enzyme on the interaction between enzyme and substrate, MM-PBSA analysis was performed to calculate the binding energy [24]. For each complex, the van der Waals energy (Evdw), electrostatic energy (Eelec), polar solvation energy (Gpolar), non-polar solvation energy (G-nonpol), and binding free energy (ΔG binding) are calculated and presented in Table 3. The results showed that ΔG binding of all mutant complexes is higher than the native complex, indicating the positive effect of applied mutations on increasing enzyme activity and substrate binding. Likewise, based on separate components, binding, van der Waals, electrostatic, and polar solvation energies in A176V and L184M complexes are more than the natural complex and, thus, are desirable for stronger binding of the ligand to the enzyme because they have higher negative values. On the other hand, the energy value of APolar solvation is positive, thus preventing the formation of complexes (Table 3). Among these components, the most impact on binding energy is related to Polar solvation energy (Table 3). The significant difference between the binding energy components of the complexes is seen in the van der Waals energy, which in the A176V and L184M complexes is 3.54 and 3.24 times more than the native complex, respectively (Table 3).

Table 3. Binding free energy and its components of paraoxon with native and mutated OPH calculated with MM-PBSA (Unit: kJ/mol).

Complexes	van der Waals Energy	Electrostatic Energy	Polar Solvation Energy	APolar Solvation Energy	Binding Energy
Native	-35.42	-18.42	-9887.03	344.34	-9595
A176V	-125.51	-23.79	-9973.38	351.62	-9770
L184M	-115.07	-22.87	-10335.56	355.74	-10117

3.9. Effect of mutations on the enzyme structure and activity.

Loops are important parts of protein structure due to their high flexibility; thus, modification of loops has been considered in protein engineering [41]. Studies have shown that mutations in loop 4 (171-178 aa) of the OPH can be useful in altering the catalytic activity of

this enzyme. For instance, the Thr172Ala and Thr173Ala mutants have improved the activity of this enzyme for the V-type nerve agent [42]. Based on the analysis, Ala176 was selected for mutation. In the native enzyme, Ala176 has a conventional hydrogen bond with a length of 2.42Å with Gln211 and a carbon-hydrogen bond with a length of 2.42Å with Gln180. In the A176V, the conventional hydrogen bond length between Val176 and Gln211 and the carbon-hydrogen bond length between Val176 and Gln180 are reduced to 1.92 and 1.93Å, respectively. The important point is forming a carbon-hydrogen bond between Val176 and Thr172 with a length of 2.72Å, which does not exist in the native enzyme between Ala176 and Thr172 (Figure 6). In the native enzyme, Gly174 has a hydrogen bond with Asp108. It has been found that the removal of this bond reduces enzyme activity due to decreased stability of the enzyme structure [43, 44]. In the A176V, in addition to the hydrogen bond between Gly174 and Asp108, a 2.89-length Å hydrogen bond is formed between Thr172 and Asp108. On the other hand, the hydrogen bond between Thr172 and Gln212, which is present in the structure of the native enzyme, has been removed by the A176V mutation (Figure 6). These results indicate that A176V mutation can have a positive effect on OPH activity by changing the pattern of hydrogen bonds.

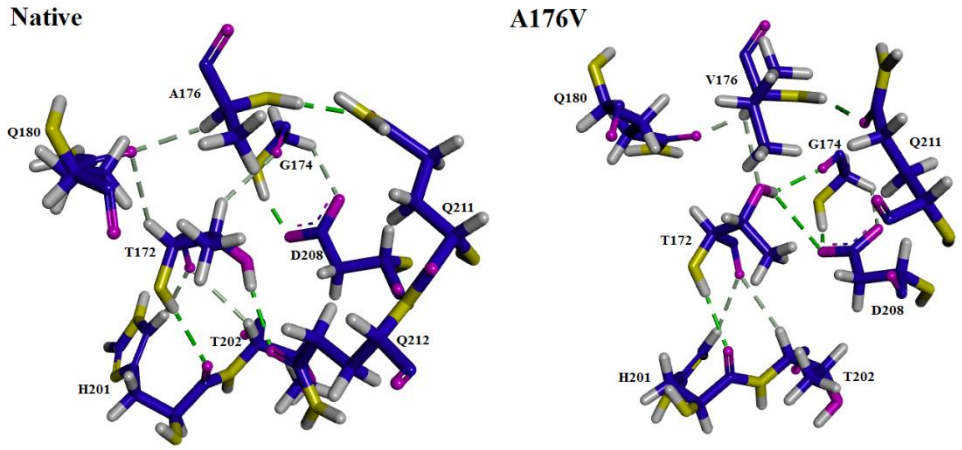

Figure 6. Comparison of the inter-atomic interaction in the native and A176V form. All the intra-conventional hydrogen bonds with the neighboring residues are shown in green dotted lines, whereas gray dotted lines signify carbon-hydrogen bonds.

Based on the HSSP results, at 184 position, the L184M mutation was selected. It has already been determined that Thr172 in loop 4 is in close contact with the Leu184 side-chain in Helix 4, and the F216L mutation with an indirect effect on this residue as well as a slight increase in the fluctuation of Thr172 and Thr173 residues increased 50% of OPH kinetic efficiency [45]. In the native enzyme, the side-chain distance between Thr172 and Leu184 is 4.228Å. Methionine has a longer side chain than leucine; thus, the distance between the side chains of Thr172 and Met184 in the L184M structure has been reduced to 3.028 angstroms (Figure 7). On the other hand, MD results showed that the RMSF values of the residues Thr172 and Thr173 in the native complex are 0.099 and 0.165nm, respectively (Figure 7). In the L184M complex, the RMSF value of the Thr172 residue is 0.075, and the Thr173 residue is 0.173nm. It can be concluded that the effect of L184M mutation in shortening the side-chain distance of M184 and Thr172 residues and also the change in the fluctuation of Thr172 and Thr173 residues are very similar to F216L mutation and is confirmed by MM-PBSA analysis. According to the results of MM-PBSA, the L184M mutation increased the ΔG binding (higher negative value) of the enzyme, indicating the positive effect of the applied mutation.

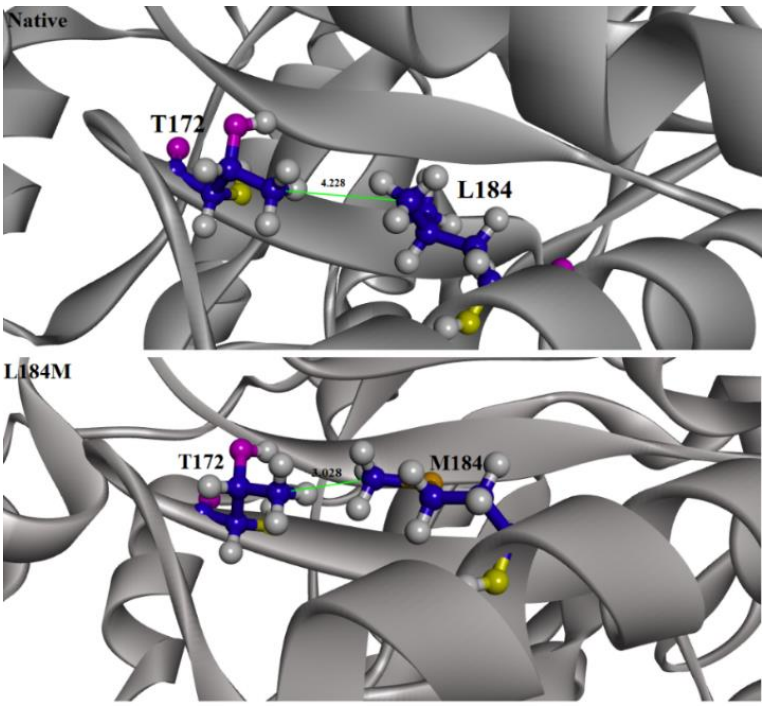

Figure 7. Comparison of the inter-atomic interaction in the native and L184M form. The distance between Thr172 and Leu184 (in native) and Thr172 and Met184 (L184M) is shown in the green line.

4. Conclusions

The ability of the *Brevundimonas diminuta* OPH to degrade a wide range of organophosphate compounds has made it an important target in the production of enzymes with high catalytic efficiency against OP compounds. In the current study, 176 and 184 positions of OPH were selected to increase its activity in paraoxon degradation. Therefore, A176V and L184M mutants were generated, and then the effect of these mutations on OPH activity was investigated based on *in silico* methods. Based on the RMSD and Rg profiles obtained from MD simulations, the applied mutations do not hurt the stability and rigidity of the enzyme, and the enzyme-ligand complexes are stable in them, confirming the molecular docking results. On the other hand, the observed changes in RMSF may indicate a stronger interaction of some residues with ligands in mutant structures. A maximum of 3 H-bonds was formed between paraoxon and enzyme in the three studied complexes. The MM-PBSA analysis showed that the applied mutations reduced ΔG binding and increased affinity, and Polar solvation energy played the most important role in this increase. It seems that A172V affects OPH activity mutation by changing the hydrogen bonding network of residues such as Gly174, Thr172, and Asp108, while L184M mutation increases OPH affinity to paraoxon by changing the fluctuation of Thr172 and Thr173 residues and getting closer to the side-chain of Met184 and Thr172. This is the first report revealing that mutation in positions 176 and 184 can increase OPH activity to paraoxon. Finally, it should be noted that validation of the results of the *in silico* analyses requires experimental studies to determine the exact effect of these mutations on enzyme activity.

Funding

This research received no external funding.

Acknowledgments

The authors thank the Research Council of Baqiyatallah University of Medical Sciences for their kind help. It should be noted that this paper was extracted from the research project of the Applied Biotechnology Research Center, Baqiyatallah University of Medical Sciences, Tehran, Iran.

Conflicts of Interest

The authors declare no conflict of interest.

References

1. Jiang, B.; Zhang, N.; Xing, Y.; Lian, L.; Chen, Y.; Zhang, D.; Li, G.; Sun, G.; Song, Y. Microbial degradation of organophosphorus pesticides: novel degraders, kinetics, functional genes, and genotoxicity assessment. *Environ. Sci. Pollut. Res.* **2019**, *26*, 21668-21681, https://doi.org/10.1007/s11356-019-05135-9.
2. Ireland, D.; Rabeler, C.; Gong, T.; Collins, E.-M.S. Bioactivation and detoxification of organophosphorus pesticides in freshwater planarians shares similarities with humans. *Arch. Toxicol.* **2022**, *96*, 3233-3243, https://doi.org/10.1101/2022.06.20.496885.
3. Poirier, L.; Jacquet, P.; Plener, L.; Masson, P.; Daudé, D.; Chabrière, E. Organophosphorus poisoning in animals and enzymatic antidotes. *Environ. Sci. Pollut. Res.* **2021**, *28*, 25081-25106, https://doi.org/10.1007/s11356-018-2465-5.
4. Chen, J.; Guo, Z.; Zhang, H.; Xin, Y.; Shi, Y.; Gu, Z.; Zhang, L.; Zhong, J.; Guo, X.; Li, Y.; Shi, G. Development of a multimetal-based phosphotriesterase hybrid nanoflowers for decontamination of environmental organophosphorus compounds pollution. *Chem. Eng. J.* **2022**, *446*, 136933, https://doi.org/10.1016/j.cej.2022.136933.
5. Iyengar, A.R.S.; Pande, A.H. Organophosphate-Hydrolyzing Enzymes as First-Line of Defence Against Nerve Agent-Poisoning: Perspectives and the Road Ahead. *Protein J.* **2016**, *35*, 424-439, https://doi.org/10.1007/s10930-016-9686-6.
6. Iyer, R.; Iken, B. Protein engineering of representative hydrolytic enzymes for remediation of organophosphates. *Biochem. Eng. J.* **2015**, , 134-144, https://doi.org/10.1016/j.bej.2014.11.010.
7. Schofield, D.A.; DiNovo, A.A. Generation of a mutagenized organophosphorus hydrolase for the biodegradation of the organophosphate pesticides malathion and demeton-S. *J. Appl. Microbiol.* **2010**, *109*, 548-557, https://doi.org/10.1111/j.1365-2672.2010.04672.x.
8. Zheng, X.; Wang, L.; Qi, L.; Dong, Z. A Novel Organophosphorus Acid Anhydrolase from Deep Sea Sediment with High Degradation Efficiency for Organophosphorus Pesticides and Nerve Agent. *Microorganisms* **2022**, *10*, 1112, https://doi.org/10.3390/microorganisms10061112.
9. Rouhani, M.; Khodabakhsh, F.; Norouzian, D.; Cohan, R.A.; Valizadeh, V. Molecular dynamics simulation for rational protein engineering: Present and future prospectus. *J. Mol. Graph. Model.* **2018**, *84*, 43-53. https://doi.org/10.1016/j.jmgm.2018.06.009.
10. Ramírez D. Computational Methods Applied to Rational Drug Design. *Open J. Med. Chem.* **2016**, *10*, 7, https://doi.org/10.2174/1874104501610010007.
11. Zhu, J.; Li, X.; Zhang, S.; Ye, H.; Zhao, H.; Jin, H.; Han, W. Exploring stereochemical specificity of phosphotriesterase by MM-PBSA and MM-GBSA calculation and steered molecular dynamics simulation. *J. Biomol. Struct. Dyn.* **2017**, *35*, 3140-3151, https://doi.org/10.1080/07391102.2016.1244494.
12. Mirzaei, M.; Latifi, AM.; Jafari, R. Improvement of Thermal Stability of DFPase by *In silico* Methods. *J. Appl. Biotechnol. Rep.* **2014**, *1*, 155-159.
13. Mohammadi, M.; Sakhteman, A.; Ahrari, S.; Hassanpour, K.; Hashemi, S.E.; Farnoosh, G. Disulfide bridge formation to increase thermostability of DFPase enzyme: A computational study. *Comput. Biol. Chem.* **2018**, *77*, 272-278, https://doi.org/10.1016/j.compbiolchem.2018.09.005.
14. Farnoosh, G.; Khajeh, K.; Latifi, A.M.; Aghamollaei, H. Engineering and introduction of *de novo* disulphide bridges in organophosphorus hydrolase enzyme for thermostability improvement. *J. Biosci.* **2016**, *41*, 577-588, https://doi.org/10.1007/s12038-016-9643-8.
15. El Khoury, L.; Mobley, D.L.; Ye, D.; Rempe, S.B. Enhancing Paraoxon Binding to Organophosphorus Hydrolase Active Site. *Int. J. Mol. Sci.* **2021**, *22*, 12624, https://doi.org/10.3390/ijms222312624.

16. Chen, J.; Luo, X.-J.; Chen, Q.; Pan, J.; Zhou, J.; Xu, J.-H. Marked enhancement of *Acinetobacter* sp. organophosphorus hydrolase activity by a single residue substitution Ile211Ala. *Bioresour. Bioprocess.* **2015**, *2*, 39, https://doi.org/10.1186/s40643-015-0067-3.
17. Dodge, C.; Schneider, R.; Sander, C. The HSSP database of protein structure—sequence alignments and family profiles. *Nucleic Acids Res.* **1998**, *26*, 313-315, https://doi.org/10.1093/nar/26.1.313.
18. Webb, B.; Sali, A. Protein Structure Modeling with MODELLER. In: Functional Genomics. Methods in Molecular Biology, Kaufmann, M.; Klinger, C.; Savelsbergh, A., Eds.; Humana Press, New York, NY. **2017**, Volume 1654, 39-54, https://doi.org/10.1007/978-1-4939-7231-9_4.
19. Kim, S.; Thiessen, P.A.; Bolton, E.E.; Chen, J.; Fu, G.; Gindulyte, A.; Han, L.; He, J.; He, S.; Shoemaker, B.A.; Wang, J.; Yu, B.; Zhang, J.; Bryant, S.H. PubChem Substance and Compound Databases. *Nucleic Acids Res.* **2016**, *44*, D1202-D1213, https://doi.org/10.1093/nar/gkv951.
20. Forli, S.; Huey, R.; Pique, M.E.; Sanner, M.F.; Goodsell, D.S.; Olson, A.J. Computational protein–ligand docking and virtual drug screening with the AutoDock suite. *Nat. Protoc.* **2016**, *11*, 905-919, https://doi.org/10.1038/nprot.2016.051.
21. Laskowski, R.A.; Swindells, M.B. LigPlot+: Multiple Ligand–Protein Interaction Diagrams for Drug Discovery. *J. Chem. Inf. Model* **2011**, *51*, 2778-2786. https://doi.org/10.1021/ci200227u.
22. Abraham, M.J.; Murtola, T.; Schulz, R.; Páll, S.; Smith, J.C.; Hess, B.; Lindahl, E. GROMACS: High performance molecular simulations through multi-level parallelism from laptops to supercomputers. *SoftwareX* **2015**, *1-2*, 19-25, https://doi.org/10.1016/j.softx.2015.06.001.
23. Kollman, P.A.; Massova, I.; Reyes, C.; Kuhn, B.; Huo, S.; Chong, L.; Lee, M.; Lee, T.; Duan, Y.; Wang, W.; Donini, O.; Cieplak, P.; Srinivasan, J.; Case, D.A.; Cheatham, T.E. Calculating Structures and Free Energies of Complex Molecules: Combining Molecular Mechanics and Continuum Models. *Acc. Chem. Res.* **2000**, *33*, 889-897, https://doi.org/10.1021/ar000033j.
24. Kumari, R.; Kumar, R. Open Source Drug Discovery Consortium, Lynn A. *g_mmpbsa*-A GROMACS Tool for High-Throughput MM-PBSA Calculations. *J. Chem. Inf. Model.* **2014**, *54*, 1951-1962, https://doi.org/10.1021/ci500020m.
25. Pagadala, N.S.; Syed, K.; Tuszynski, J. Software for molecular docking: a review. *Biophys. Rev.* **2017**, *9*, 91-102, https://doi.org/10.1007/s12551-016-0247-1.
26. Tao, X.; Huang, Y.; Wang, C.; Chen, F.; Yang, L.; Ling, L.; Che, Z.; Chen, X. Recent developments in molecular docking technology applied in food science: a review. *Int. J. Food Sci. Technol.* **2020**, *55*, 33-45, https://doi.org/10.1111/ijfs.14325.
27. Morris, G.M.; Huey, R.; Lindstrom, W.; Sanner, M.F.; Belew, R.K.; Goodsell, D.S.; Olson, A.J. AutoDock4 and AutoDockTools4: Automated docking with selective receptor flexibility. *J. Comput. Chem.* **2009**, *30*, 2785-2791, https://doi.org/10.1002/jcc.21256.
28. Morris, G.M.; Huey, R.; Olson, A.J. Using AutoDock for Ligand-Receptor Docking. *Curr. Protoc. Bioinformatics* **2008**, *24*, 8.14.1-8.14.40, https://doi.org/10.1002/0471250953.bi0814s24.
29. Zhan, D.; Zhou, Z.; Guan, S.; Han, W. The Effect of Conformational Variability of Phosphotriesterase upon N-acyl-L-homoserine Lactone and Paraoxon Binding: Insights from Molecular Dynamics Studies. *Molecules* **2013**, *18*, 15501-15518, https://doi.org/10.3390/molecules181215501.
30. Raval, K.; Ganatra, T. Basics, types and applications of molecular docking: A review. *IP Int. J. Compr. Adv. Pharmacol.* **2022**, *7*, 12-16, https://doi.org/10.18231/j.ijcaap.2022.003.
31. Guo, J.; Gan, C.; Cheng, B.; Cui, B.; Yi, F. Exploration of binding mechanism of apigenin to pepsin: Spectroscopic analysis, molecular docking, enzyme activity and antioxidant assays. *Spectrochim. Acta A Mol. Biomol. Spectrosc.* **2023**, *290*, 122281, https://doi.org/10.1016/j.saa.2022.122281.
32. Manandhar, S.; Sankhe, R.; Priya, K.; Hari, G.; Kumar, H.B.; Mehta, C.H.; Nayak, U.Y.; Pai, K.S.R. Molecular dynamics and structure-based virtual screening and identification of natural compounds as Wnt signaling modulators: possible therapeutics for Alzheimer's disease. *Mol. Divers.* **2022**, *26*, 2793-2811, https://doi.org/10.1007/s11030-022-10395-8.
33. Mahmood, A.; Samad, A.; Shah, A.A.; Wadood, A.; Alkathiri, A.; Alshehri, M.A.; Alam, M.Z.; Hussain, T.; He, P.; Umair, M. A novel biallelic variant in the Popeye domain-containing protein 1 (POPDC1) underlies limb girdle muscle dystrophy type 25. *Clin. Genet.* **2023**, *103*, 219-225, https://doi.org/10.1111/cge.14238.
34. Khan, M.T.; Rehaman, A.U.; Junaid, M.; Malik, S.I.; Wei, D.-Q. Insight into novel clinical mutants of RpsA-S324F, E325K, and G341R of *Mycobacterium tuberculosis* associated with pyrazinamide resistance. *Comput. Struct. Biotechnol. J.* **2018**, *16*, 379-387, https://doi.org/10.1016/j.csbj.2018.09.004.

35. Sangeetha, B.; Krishnamoorthy, A.S.; Sharmila, D.J.S.; Renukadevi, P.; Malathi, V.G.; Amirtham, D. Molecular modelling of coat protein of the *Groundnut bud* necrosis tospovirus and its binding with Squalene as an antiviral agent: In vitro and in silico docking investigations. *Int. J. Biol. Macromol.* **2021**, *189*, 618-634, https://doi.org/10.1016/j.ijbiomac.2021.08.143.
36. Zhan, D.; Guan, S.; Jin, H.; Han, W.; Wang, S. Stereoselectivity of phosphotriesterase with paraoxon derivatives: a computational study. *J. Biomol. Struct. Dyn.* **2016**, *34*, 600-611, https://doi.org/10.1080/07391102.2015.1046937.
37. Gupta, S.; Rao, A.R.; Varadwaj, P.K.; De, S.; Mohapatra, T. Extrapolation of Inter Domain Communications and Substrate Binding Cavity of Camel HSP70 1A: A Molecular Modeling and Dynamics Simulation Study. *PloS One* **2015**, *10*, e0138961, https://doi.org/10.1371/journal.pone.0136630.
38. Lobanov, M.Y.; Bogatyreva, N.S.; Galzitskaya, O.V. Radius of gyration as an indicator of protein structure compactness. *Mol. Biol.* **2008**, *42*, 623-628, https://doi.org/10.1134/S0026893308040195.
39. Williams, D.H.; Stephens, E.; O'Brien, D.P.; Zhou, M. Understanding Noncovalent Interactions: Ligand Binding Energy and Catalytic Efficiency from Ligand-Induced Reductions in Motion within Receptors and Enzymes. *Angew. Chem. Int. Ed.* **2004**, *43*, 6596-6616, https://doi.org/10.1002/anie.200300644.
40. Shamsi, A.; Shahwan, M.; Khan, M.S.; Alhumaydhi, F.A.; Alsagaby, S.A.; Al Abdulmonem, W.; Abdullaev, B.; Yadav, D.K. Mechanistic Insight into Binding of Huperzine A with Human Serum Albumin: Computational and Spectroscopic Approaches. *Molecules* **2022**, *27*, 797, https://doi.org/10.3390/molecules27030797.
41. Rahban, M.; Zolghadri, S.; Salehi, N.; Ahmad, F.; Haertlé, T.; Rezaei-Ghaleh, N.; Sawyer, L.; Saboury, A.A. Thermal stability enhancement: Fundamental concepts of protein engineering strategies to manipulate the flexible structure. *Int. J. Biol. Macromol.* **2022**, *214*, 642-654, https://doi.org/10.1016/j.ijbiomac.2022.06.154.
42. Jeong, Y.S.; Choi, J.M.; Kyeong, H.-H.; Choi, J.-Y.; Kim, E.-J.; Kim, H.-S. Rational design of organophosphorus hydrolase with high catalytic efficiency for detoxifying a V-type nerve agent. *Biochem. Biophys. Res. Commun.* **2014**, *449*, 263-267, https://doi.org/10.1016/j.bbrc.2014.04.155.
43. Jackson, C.J.; Foo, J.-L.; Tokuriki, N.; Afriat, L.; Carr, P.D.; Kim, H.-K.; Schenk, G.; Tawfik, D.S.; Ollis, D.L. Conformational sampling, catalysis, and evolution of the bacterial phosphotriesterase. *Proc. Natl. Acad. Sci.* **2009**, 106, 21631-21636, https://doi.org/10.1073/pnas.0907548106.
44. Yang, H.; Carr, P.D.; McLoughlin, S.Y.; Liu, J.W.; Horne, I.; Qiu, X.; Jeffries, C.M.J.; Russell, R.J.; Oakeshott, J.G.; Ollis, D.L. Evolution of an organophosphate-degrading enzyme: a comparison of natural and directed evolution. *Protein Eng. Des. Sel.* **2003**, *16*, 135-145, https://doi.org/10.1093/proeng/gzg013.
45. Olsen, A.J.; Halvorsen, L.A.; Yang, C.-Y.; Ventura, R.B.; Yin, L.; Renfrew, P.D.; Bonneau, R.; Montclare, J.K. Impact of phenylalanines outside the dimer interface on phosphotriesterase stability and function. *Mol. BioSyst.* **2017**, *13*, 2092-2106, https://doi.org/10.1039/C7MB00196G.